Large-Sized Crystal Growth and Electric-Elastic Properties of α-BaTeMo 2 O 9 Single Crystal

ARTICLE *in* CRYSTAL GROWTH & DESIGN · FEBRUARY 2015

Impact Factor: 4.89 · DOI: 10.1021/cg501574e

6 AUTHORS, INCLUDING:

Zeliang Gao

Shandong University

32 PUBLICATIONS **241** CITATIONS

SEE PROFILE

Xiangxin Tian

Shandong University

5 PUBLICATIONS **3** CITATIONS

SEE PROFILE

Junjie Zhang

Argonne National Laboratory

23 PUBLICATIONS **181** CITATIONS

SEE PROFILE

CRYSTAL GROWTH & DESIGN

Article

pubs.acs.org/crystal

Large-Sized Crystal Growth and Electric-Elastic Properties of α-$BaTeMo_2O_9$ Single Crystal

Zeliang Gao,[†] Xiangxin Tian,[†] Junjie Zhang,[†] Qian Wu,[†] Qingming Lu,[‡] and Xutang Tao*,[†]

[†]State Key Laboratory of Crystal Materials, and [‡]School of Chemistry and Engineering, Shandong University, Jinan, 250100, China

ABSTRACT: Bulk crystal of α-$BaTeMo_2O_9$ with dimensions up to 90 × 38 × 27 mm^3 was grown successfully by a top-seeded solution growth method. In the crystal growth process, a low cooling rate (0.1−0.5 °C/day) and dynamic adjustment of rotating speed were adopted in order to stabilize the metastable growth and improve the crystal quality. The crystal facets {002}, {010}, {20$\bar{1}$}, {111} are in good accordance with the predicted growth morphology based on the Bravais−Friedel and Donnay−Harker method. The complete sets of the dielectric, elastic, and piezoelectric constants of the α-$BaTeMo_2O_9$ crystals have been determined by means of the resonant technique and impedance analysis at room temperature. The results show that the α-$BaTeMo_2O_9$ crystal possesses much smaller piezoelectric constants (d_{31} = −1.8 pm/V, d_{15} = 4.9 pm/V, and d_{31} = 0.3 pm/V) than that of β-$BaTeMo_2O_9$. In addition, the structural distortions and dipole moments of α-$BaTeMo_2O_9$ and β-$BaTeMo_2O_9$ were analyzed and calculated to explain the obvious differences upon the properties between the two crystals.

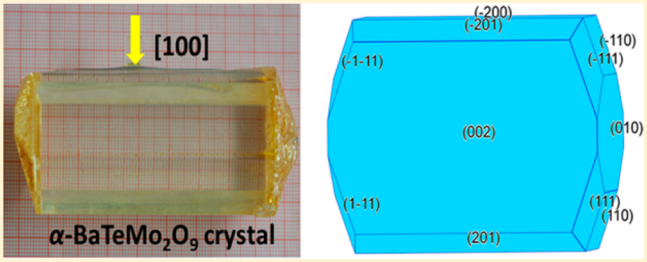

INTRODUCTION

Oxide single crystals have played more and more important roles in the modern scientific research and applications since they have relative good growth habits, stability, and excellent physical properties. Up to now, the oxide crystals such as SiO_2, $LiNbO_3$, $KTiOPO_4$ (KTP), KH_2PO_4 (KDP), LiB_3O_5 (LBO), β-BaB_2O_4 (BBO), $KBe_2BO_3F_2$ (KBBF), $BaWO_4$, and YVO_4, etc., have been widely used in electrical and optical fields.[1−9] Recently, the design and synthesis of the non-centrosymmetric inorganic oxides under the guidance of the second-order Jahn−Teller effects (SOJT) have attracted great interest, due to their excellent properties of piezoelectricity, pyroelectricity, ferroelectricity, stimulated Raman scattering, and second-order nonlinear optical activity.[10−16] These materials usually contain distorted MO_6 octahedra (M = Mo^{6+} or W^{6+}) and AO_xE polyhedra (A = Te^{4+} or Se^{4+} with stereochemically active lone pairs, and E = lone pair).[10−13] In these materials, the octahedral coordinate M cations can be distorted toward an edge (C_2), face (C_3), or corner (C_4) of a MO_6 octahedron.[17,18] Because of the impact from the lone pairs, the oxide ligands move toward one single side of the cation in the AO_xE polyhedra, leading to the non-centrosymmetry exhibition of the crystal structure, which results in the piezoelectric, electro-optical, and second-order nonlinear optical properties. Therefore, compounds such as β-$BaTeMo_2O_9$ (β-BTM), $BaTeW_2O_9$, $Na_2TeW_2O_9$, $Cs_2TeMo_3O_{12}$, $Na_2Te_3Mo_3O_{12}$, and $Ag_2Te_3Mo_3O_{16}$ with high second-harmonic generation efficiencies have been synthesized.

To study the physical properties of these materials, our group has poured much effort into and obtained fruitful results in developing the single crystal growth.[12,14−16,19] To date, bulk single crystals of β-BTM, $BaTeW_2O_9$, and $Cs_2TeMo_3O_{12}$ have been grown by the top-seeded solution growth (TSSG) slow-cooling method using TeO_2−MoO_3 or TeO_2−WO_3 fluxes. These materials are not only good candidates as nonlinear optical crystals but also as piezoelectric and Raman crystals.[16,19] In the course of growing of β-BTM, another novel material α-$BaTeMo_2O_9$ (α-BTM) was identified.[20] The structure analysis indicates that it crystallizes in the orthorhombic space group $Pca2_1$ (No. 29) with cell parameters a = 14.8683(2) Å, b = 5.6636(1) Å, c = 17.6849(3) Å, and Z = 8. The irreversible phase transition from β-BTM to α-BTM was been discovered by Zhang and Marczka, respectively.[20,21] Under the same conditions, the powder second-harmonic generation of α-BTM (0.2 × KDP) is much smaller than that of β-BTM (about 2.5 × KDP).[20] The Z-scan analysis show that β-BTM possess promising third-order optical susceptibilities, and it means that α-BTM would also exhibit similar properties.[22] The Raman spectra of α-BTM and β-BTM have been determined, calculated, and analyzed in detail.[19,23,24] It is worth to noting that both α-BTM and β-BTM are high efficiency stimulated Raman scattering materials.[19,25] Since the long crystal is beneficial for the high efficiency nonlinear outputs, the α-BTM crystals with large dimensions are great interesting.

In this paper, the TeO_2−MoO_3 mixture flux was optimized, and the growth of α-BTM with dimensions up to 90 × 38 × 27 mm^3 was reported. Its electrical properties including elastic, dielectric, and piezoelectric properties were also determined at room temperature. Furthermore, the structural distortions of both α-BTM and β-BTM were analyzed and compared to explain the difference of their piezoelectric property.

Received: October 24, 2014
Revised: December 16, 2014
Published: December 22, 2014

DOI: 10.1021/cg501574e
Cryst. Growth Des. 2015, 15, 759−763

EXPERIMENTAL SECTION

Crystal Growth. In 2011, our group reported the synthesis and bulk crystal growth of α-BTM (51 × 30 × 20 mm^3, Figure 1a) with a seed crystal oriented along the [010] direction for the first time.[26] Different from the former experiment parameters, the flux system is optimized, and a crystal seed along the [100] direction is used in this experiment. It is well-known that solution with high viscosity is not attractive for crystal growth because it makes the growth time-consuming and gives rise to the possibility of the occurrence of inclusion and concentration of ionic impurity in the crystal. In the research of flux optimization, we found lower concentration, and more TeO_2 in the flux can reduce the viscosity of the solution. Therefore, the ratio of the mixture of TeO_2−MoO_3 flux was changed from 6:5 to 3:2, which can reduce the viscosity of the solution. Two equivalent ways can be adopted to prepare the high temperature solution. One is to pour polycrystalline α-BTM (2.40 mol) to the mixture of TeO_2−MoO_3 (TeO_2 6.35 mol, MoO_3 4.24 mol) at 650 °C in a platinum crucible placed in the constant temperature region of a vertical furnace, and a process of stirring for 24 h was followed to form homogeneous solution. The other way is to heat the mixed powders of $BaCO_3$ (2.40 mol), TeO_2 (8.75 mol), and MoO_3 (9.04 mol) in a platinum crucible slowly to 650 °C, and the process of stirring for 24 h was also employed. The furnace temperature was measured by a Pt−Rh thermocouple and controlled by Yudian AI-808P controller/programmer. To research the relations between the seed crystal direction and crystal growth habit, a crystal seed along the [100] direction was used in this work. It was attached with platinum wire to an alumina rod. After the saturation temperature was determined, slowly the temperature was decreased from 650 to 20 °C above the saturation point and the crystal seed was slightly dipped into the solution. The solution was then cooled to the saturation temperature in 6 h.

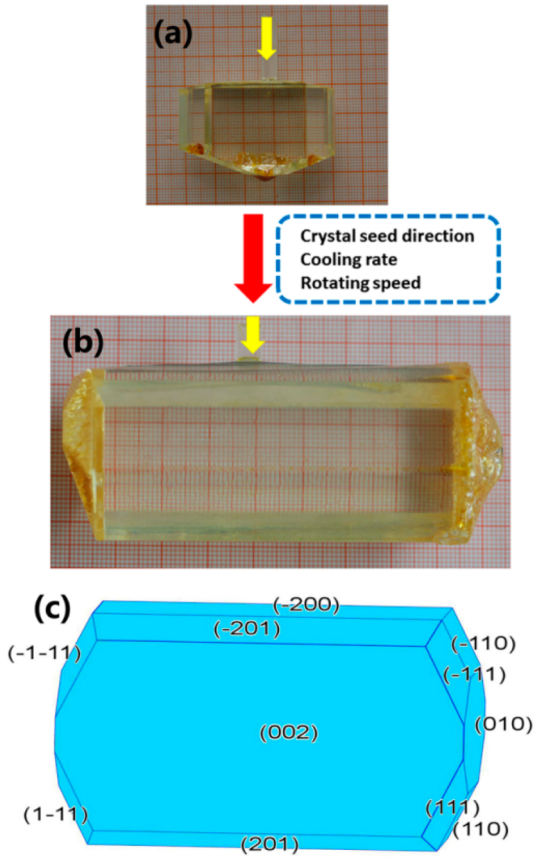

Figure 1. (a) Photograph of the α-BTM crystal with growth direction [010]. (b) Photograph of the α-BTM crystal with growth direction [100]. (c) Predicted growth morphology of α-BTM crystal based on the BFDH method.

It is worth to note that a lower cooling rate and dynamic adjustment of rotating speed during the growth were adopted in order to stabilize the metastable growth and improve the crystal quality. Then the solution was cooled at a very low rate of 0.1−0.5 °C/day, while the former rate was 0.25−0.5 °C/day. At the beginning of the growth, the seed crystal rotated at 32 rpm at the center of the solution, and the rotation speed was slowly changed to 15 rpm as bulk crystal was being grown. When the growth was ended, the single crystal was pulled up and hung over the surface of solution and cooled at a rate of 5−10 °C/h to room temperature. Figure 1 shows the as-grown α-BTM crystal.

Dielectric Properties. According to the IEEE standard, the relations between the electrical coordinate axes and crystallographic axes can be expressed as a//X, b//Y, and c//Z for α-BTM. The dielectric property can be expressed with a second-order tensor, and there are three independence dielectric constants ε_{11}, ε_{22}, ε_{33}. The dielectric property can be determined with samples X-, Y-, and Z-square samples. In our experiment, the dimensions of these samples are 6 × 6 × 2 mm^3. Then, all the dielectric constants can be obtained from the measured capacitance values at 1 kHz using the following formula:

$$\varepsilon_{ii} = \frac{c_{ii}t}{A\varepsilon_0}\bigg| i = 1, 2, 3 \tag{1}$$

where c is the capacitance, t is the thickness, A is the area of the sample, and ε_0 is the vacuum dielectric constant.

Elastic and Piezoelectric Properties. Both the elastic and piezoelectric constants can be determined by a resonance technique with an Agilent 4294A impedance network analyzer. In the electrical coordinate system, the axes X, Y, and Z form a right-handed orthogonal coordinate system, while the Z axis is along its positive direction. As a polar crystal, the positive direction of Z axis and d_{33} were determined by a quasi-static piezoelectric d_{33} meter (model ZJ-2, Institute of Acoustics Academia Sinica, Beijing, China). There are five and nine piezoelectric and elastic constants for α-BTM, and they can be obtained by 10 samples which are shown in Figure 2. These samples are divided into two kinds: non-circumgyrate (red in figure) and circumgyrate (blue in figure). As shown in Table 1, the first and second letters denote the directions of the thickness and length for all the samples. The third and fourth letters in the circumgyrate samples mean the rotation direction and rotation angle. The dimensions of the rectangular bars were typically 10 × 3.5 × 2 mm^3, and 4 × 4 × 10 mm^3 for the z bar. The dimensional variations in each sample were less than 3%. All the samples were sputter coated with silver in the electric field directions listed in Table 1. The piezoelectric constants d_{33} and elastic constants s_{33} were determined by the resonance technique using eqs 2−4. Piezoelectric constants d_{31}, d_{32} and elastic constants s_{22} and s_{11} can be obtained using eqs 4−6. The vibration modes of elastic constants s_{44}, s_{55}, s_{66} are different from that of s_{11}, s_{22}, and s_{33}. Take s_{44}

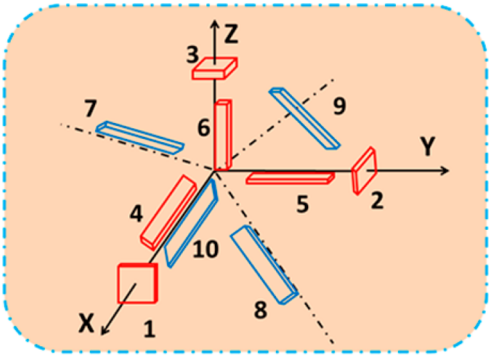

Figure 2. Schematic diagram of the samples for measuring the dielectric, elastic, and piezoelectric constants.

DOI: 10.1021/cg501574e
Cryst. Growth Des. 2015, 15, 759−763

Table 1. Elastic and Piezoelectric Constants for Different Specimens

no.	sample	electric field direction	constants
1	x square	x	s_{55}, ε_{11}
2	y square	y	s_{44}, ε_{22}
3	z square	z	ε_{33}
4	zx	z	d_{31}, s_{11}
5	zy	z	d_{32}, s_{23}
6	z bar	z	d_{33}, s_{33}
7	$zx\omega(45°)$	z/y	s_{13}, d_{15}
8	$zxt(45°)$	z	s_{12}
9	$yz\omega(45°)$	y	d_{24}, s_{23}
10	$zxl(45°)$	x	s_{66}

as an example: it can be obtained using eqs 7−8. The other piezoelectric and elastic constants including d_{15}, d_{24}, s_{12}, s_{13}, and s_{23} should be determined using circumgyrate samples. Piezoelectric constants d_{24} and d_{15} can be expressed as eqs 9 and 10 in a new coordinate system. Then the constants can be obtained with former values of constants d_{33}, d_{32}, and d_{31}. Similarly, the elastic constants s_{12}, s_{13}, and s_{23} can also be obtained. Stiffness coefficients (c_{ij}) can be obtained from the data of elastic constants using eq 11.

$$k_{33}^2 = \frac{\pi}{2}\frac{\mathrm{fr}}{\mathrm{fa}}\mathrm{tg}\left(\frac{\pi}{2}\frac{\mathrm{fa}-\mathrm{fr}}{\mathrm{fa}}\right) \tag{2}$$

$$s_{33} = \frac{1}{4\rho(\mathrm{lfa})^2(1-k^2)} \tag{3}$$

$$d_{ii} = k(\varepsilon_{ii}s_{ii})^{0.5} \tag{4}$$

$$s_{ii} = \frac{1}{4\rho(f_r l_{ii})^2} \tag{5}$$

$$\frac{k^2}{1-k^2} = \frac{\pi f_a}{2}\cot\frac{\pi}{2}\left(\frac{f_r}{f_a}\right) \tag{6}$$

$$\frac{s_{44}}{F^2} = \frac{1}{4\rho(f_r l)^2} \tag{7}$$

$$F = 1.2916 - 0.0458\sqrt{\frac{s_{22}+s_{33}}{s_{44}}} \tag{8}$$

$$d'_{22} = d_{33}\sin^3\theta + d_{32}\sin\theta\cos^2\theta + \frac{1}{2}d_{24}\cos\theta\sin(2\theta) \tag{9}$$

$$d'_{33} = d_{33}\cos^3\theta + d_{31}\cos\theta\sin^2\theta + \frac{1}{2}d_{15}\sin\theta\sin(2\theta) \tag{10}$$

$$c = s^{-1} \tag{11}$$

RESULTS AND DISCUSSION

Crystal Growth. The bulk α-BTM crystal with dimensions of 90 × 38 × 27 mm^3 grown by the TSSG method using an a-axis oriented seed is shown in Figure 1. It is obvious that the morphology is different from that of the crystal usinga b-axis oriented seed. Using the X-ray crystal orientation apparatus, the indices of the distinguishable facets were determined as {002}, {010}, {20$\bar{1}$}, {111}. The theoretical morphology of the crystal is established by using the Materials Studio Modeling grogram with its structural parameters, according to the Bravais−Friedel and Donnay−Harker (BFDH) methods. As shown in Figure 1b,c, the distinguishable facets are in good accordance with the predicted growth morphology. As shown in Figure 1b, there are many mixtures of TeO_2−MoO_3 that adhere to both ends of the crystal, and many predicted facets have not been shown here. With a better progress for pulling of the crystal out of the furnace, these no-reveal facets should be observed. According to the morphology analysis, it can be seen that the crystal grows much more quickly along the [010] direction than in the other directions, and a long crystal can be obtained with crystal seeds along the [100] direction.

Elastic and Piezoelectric Properties. The elastic and piezoelectric constants are listed in Table 2. It can be seen that the elastic property exhibits small anisotropy with s_{11} = 16.70

Table 2. Dielectric, Elastic, and Piezoelectric Coefficients of α-$BaTeMo_2O_9$ Crystal

Elastic Coefficients s_{ij} (pm^2/N)													
	s_{11}	s_{22}	s_{33}	s_{44}	s_{55}	s_{66}	s_{12}	s_{13}	s_{15}	s_{23}	s_{25}	s_{35}	s_{46}
α-BTM	16.70	12.10	13.88	14.36	26.42	18.94	7.69	−2.83		4.48			
β-BTM	11.47	10.96	14.42	36.46	32.78	26.80	−3.64	−2.72	0.12	−2.47	−0.11	0.54	3.13
SiO_2	12.77		9.60	20.04		29.12	−0.29	−1.22					
Piezoelectric Coefficients d_{ij}(pC/N)													
	d_{31}	d_{32}	d_{33}	d_{15}	d_{24}	d_{14}	d_{16}	d_{22}	d_{23}	d_{25}	d_{34}	d_{36}	d_{11}
α-BTM	−1.8	−1.8	0.3	4.9	<0.1	0	0	0	0	0	0	0	0
β-BTM	0	0	0	0	0	12.04	7.46	−10.8	3.21	−0.64	30.25	12.83	0
SiO_2	0	0	0	0	0	−0.727		0	0	0.727	0	0	−2.31
Dielectric Coefficients ε_{ij}													
	ε_{11}		ε_{22}		ε_{33}		ε_{13}						
α-BTM	14.06		29.98		16.49								
β-BTM	17.91		23.02		29.42		10.23						
SiO_2	39.97		39.97		41.03								
Shear Electromechanical Coupling Factor k_{ij}													
	k_{31}		k_{32}		k_{33}								
α-BTM	5.4%		5.0%		1.9%								
Stiffness Coefficients c_{ij} (10^{10} N/m^2)													
	c_{11}	c_{22}	c_{33}	c_{44}	c_{55}	c_{66}	c_{12}	c_{13}	c_{23}				
α-BTM	10.89	16.49	10.53	6.96	3.78	5.28	−8.8	5.06	−7.12				

DOI: 10.1021/cg501574e
Cryst. Growth Des. 2015, 15, 759−763

pm^2/N, s_{22} = 12.10 pm^2/N, and s_{33} = 13.88 pm^2/N. The piezoelectric constants (d_{31} = −1.8 pC/N, d_{32} = −1.8 pC/N, d_{15} = 4.9 pC/N, d_{33} = 0.3 pC/N) are comparable to SiO_2 (d_{11} = −2.31 pC/N, d_{14} = −0.727 pC/N). However, they are much smaller than that of β-BTM (d_{34} = 30.25 pC/N, d_{22} = 10.8 pC/N, d_{14} = 12.04 pC/N).[16]

Both α-BTM and β-BTM belong to polar crystals. In some sense, the values of longitudinal piezoelectric constants (d_{ii}, i = 1, 2, and 3) can denote their dipole moments. The piezoelectric constants d_{22} of β-BTM is two orders larger in magnitude than that of d_{33} for α-BTM. It is well-known that the piezoelectric, electro-optical, and second-order nonlinear properties intensity depend on the non-centrosymmetric structure. The huge piezoelectric differences between α-BTM and β-BTM would be explained by their crystal structures. Our previous studies show that both α-BTM and β-BTM contain distorted Mo−O_6 octahedra and Te−O_x (x = 3, 4) polyhedral.[10,20] Four and two Mo^{6+} cations located in α-BTM and β-BTM, respectively, distorted toward a face of its oxide octahedron. For α-BTM, the out-of-center distortions induce three short Mo−O bonds of 1.726−1.773 Å and three long ones of 2.107−2.293 Å. For the Te−O_4 polyhedron and Te−O_3 polyhedron, their Te−O bond distances range from 1.912 to 2.488 Å and 1.909−1.920 Å, respectively. The crystal structure of β-BTM shows that the three short Mo−O bonds are 1.721−1.826 Å, and three long ones are 2.053−2.225 Å, while the Te−O bond distances range from 1.865 to 2.348 Å in Te−O_4 polyhedron, respectively. It is worth noting that the asymmetric unit of α-BTM has the formula "$Ba_2Te_2Mo_4O_{18}$". Not only distortions in each polyhedron but also polyhedron configurations in unit cell determine the non-centrosymmetric structure. As shown in Figure 3, both the α-BTM and β-BTM exhibit two-dimensional structures, and Ba^{2+} cations are found between the layers. In the polar directions (c axis for α-BTM and b axis for β-BTM), the polyhedron distortions in α-BTM are nearly neutralized, while the polyhedron distortions in β-BTM, especially for Mo−O_6 octahedra, are superposed along the b-axis. Therefore, β-BTM possesses a much larger non-centrosymmetric structure than that of α-BTM. The magnitudes of dipole moment of Mo−O_6 octahedra and TeO_x (x = 3, 4) polyhedral in α-BTM and β-BTM are other evidence to explain their non-centrosymmetric structures. Our calculated data show that the magnitudes of dipole moments of Mo−O_6 octahedra are 372.26× 10−4 esu·cm/ $Å^3$, 390.55× 10^{-4} esu·cm/ $Å^3$, 415.84× 10^{-4} esu·cm/ $Å^3$, 437.44 × 10^{-4} esu·cm/ $Å^3$, and 312.39× 10^{-4} esu·cm/ $Å^3$, 361.71 × 10^{-4} esu·cm/$Å^3$ for α-BTM and β-BTM, respectively. Moreover, the magnitude of the dipole moment of Te−O_x (x = 3, 4) polyhedra in α-BTM and β-BTM are 663.22 × 10^{-4} esu·cm/ $Å^3$, 567.53× 10^{-4} esu·cm/ $Å^3$, and 597.44 × 10^{-4} esu·cm/ $Å^3$, respectively. It is obviously that both the magnitude of the dipole moment of Mo−O_6 octahedra and Te−O_x polyhedral in α-BTM are remarkably larger than that in β-BTM. All the directions of the dipole moments for each Mo−O_6 octahedra and Te−O_x (x = 3, 4) polyhedral are represented with blue and green arrows. As shown in Figure 3, various dipole moments point in a nearly antiparallel manner in α-BTM, while the individual dipoles align in an adductive manner in β-BTM. Then the dipole moment of the β-BTM and α-BTM unit cell is calculated to be 406.95 × 10^{-4} esu·cm/$Å^3$ and 3.73 × 10^{-4} esu·cm/$Å^3$, respectively. The above analysis is very consistent with the piezoelectric constants in our measurements.

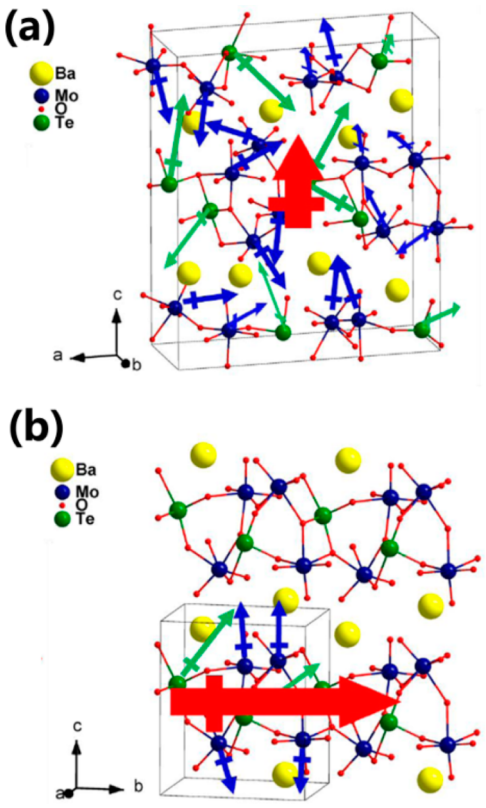

Figure 3. (a) Directions of dipole moments of each Mo−O_6 and Te−O_x (x = 3, 4) polyhedral in α-BTM. (b) Directions of dipole moments of each Mo−O_6 and Te−O_x (x = 3, 4) polyhedral in β-BTM. The blue and green arrows indicate the directions of dipole moments for Mo−O_6 and Te−O_x (x = 3, 4) polyhedra, respectively. The red arrow indicates the direction of the net dipole moments for each unit cell.

■ CONCLUSIONS

Large-sized α-$BaTeMo_2O_9$ with dimensions up to 90 × 38 × 27 mm^3 has been grown by the TSSG method. The crystal exhibits as-grown facets {002}, {010}, {20$\bar{1}$}, {111}, and they are in good accordance with the predicted growth morphology based on the BFDH method. Along the X, Y, and Z axes, the elastic constants are measured to be s_{11} = 16.70 pm^2/N, s_{22} = 12.10 pm^2/N, and s_{33} = 13.88 pm^2/N, respectively, and they possess small anisotropy. The piezoelectric coefficients of α-BTM (d_{31} = −1.8 pC/N, d_{32} = −1.8 pC/N, d_{15} = 4.9 pC/N, d_{33} = 0.3 pC/N) are comparable to that of SiO_2, but they are much smaller than that of β-BTM. Both crystal structure and dipole moment of α-BTM and β-BTM are analyzed and calculated to explain the huge piezoelectric property differences. The net dipole moment of β-BTM is two orders higher than that of α-BTM, and it is very consistent with the values of longitudinal piezoelectric constants d_{22} and d_{33}.

■ AUTHOR INFORMATION

Corresponding Author

*E-mail: txt@sdu.edu.cn.

Notes

The authors declare no competing financial interest.

■ ACKNOWLEDGMENTS

We gratefully acknowledge the financial support from the State National Natural Science Foundation of China (Grant Nos.

DOI: 10.1021/cg501574e
Cryst. Growth Des. 2015, 15, 759−763

61308088, 51021062, and 51272129), 973 Program of the People's Republic of China (Grant No. 2010CB630702), and the Program of Introducing Talents of Disciplines to Universities in China (111 Program No. b06017).

REFERENCES

(1) Brongersma, M. L.; Polman, A.; Min, K. S.; Boer, E.; Tambo, T.; Atwater, H. A. *Appl. Phys. Lett.* **1998**, *72*, 2577−2579.
(2) Myers, L. E.; Miller, G. D.; Eckardt, R. C.; Fejer, M. M. *Opt. Lett.* **1995**, *20*, 52−54.
(3) Huisken, F.; Kaloudis, M.; Marquez, J.; Chuzavkov, Y. L.; Orlov, S. N.; Polivanov, Y. N.; Smirnov, V. V. *Opt. Lett.* **1995**, *20*, 2306−2308.
(4) James, H. O.; Sliker, T. R. *J. Opt. Soc. Am.* **1964**, *54*, 1031−1040.
(5) Hall, G. J.; Ferguson, A. I. *Opt. Lett.* **1993**, *18*, 1511−1513.
(6) Degl'Innocenti, R.; Majkic, A.; Sulser, F.; Mutter, L.; Poberaj, G.; Günter, P. *Opt. Express* **2008**, *16*, 11660.
(7) Chen, C. T.; Wang, G. L.; Wang, X. Y.; Xu, Z. Y. *Appl. Phys. B: Laser Opt.* **2009**, *97*, 9−25.
(8) Cavalcante, L. S.; Sczancoski, J. C.; Lima, L. F.; Espinosa, J.; Pizani, P. S.; Varela, J. A.; Longo, E. *Cryst. Growth Des.* **2009**, *9*, 1002−1012.
(9) Huang, C. H.; Zhang, G.; Wei, M.; Huang, L. X.; Huang, X. J.; Shen, H. Y. *Opt. Commun.* **2003**, *224*, 1−4.
(10) Ra, H. S.; OK, K. M.; Halasyamani, P. S. *J. Am. Chem. Soc.* **2003**, *125*, 7764−7765.
(11) Goodey, J.; Broussard, J.; Halasyamani, P. S. *Chem. Mater.* **2002**, *14*, 3174−3180.
(12) Zhang, W. G.; Tao, X. T.; Zhang, C. Q. *Crys. Growth Des.* **2008**, *8*, 304−307.
(13) Vidyavathy, B.; Vidyasagar, K. *Inorg. Chem.* **1998**, *37*, 4764−4774.
(14) Zhang, J. J.; Tao, X. X.; Sun, Y. X.; Zhang, Z. H.; Zhang, C. Q.; Gao, Z. L.; Xia, H. B.; Xia, S. Q. *Cryst. Growth Des.* **2011**, *11*, 1863−1868.
(15) Zhang, W. G.; Li, F.; Kim, S. H. *Cryst. Growth Des.* **2010**, *10*, 4091−4095.
(16) Gao, Z. L.; Tao, X. T.; Yin, X. *Appl. Phys. Lett.* **2008**, *93* (25), 252906.
(17) Ok, K. M.; Halasyamani, P. S.; Casanova, D.; Llunell, M.; Alemany, P.; Alvarez, S. *Chem. Mater.* **2006**, *18*, 3176−3183.
(18) Bersuker, I. B. *Chem. Rev.* **2001**, *101*, 1067−1114.
(19) Gao, Z. L.; Liu, S. D.; Zhang, S. J.; Zhang, W. G.; He, J. L.; Tao, X. T. *Appl. Phys. Lett.* **2012**, *100*, 261905.
(20) Zhang, J. J.; Zhang, Z. H.; Zhang, W. G.; Zheng, Q. X.; Sun, Y. X.; Zhang, C. Q.; Tao, X. T. *Chem. Mater.* **2011**, *23*, 3752−3761.
(21) Maczka, M.; Freire, P. T. C.; Majchrowski, A.; Pizani, P. S.; Kityk, I. V. *J. Alloy. Compd.* **2013**, *579*, 236−242.
(22) Fuks-Janczarek, I.; Miedzinski, R.; Brik, M. G.; Majchrowski, A.; Jaroszewicz, L. R.; Kityk, I. V. *Solid State Sci.* **2014**, *27*, 30−35.
(23) Maczka, M.; Majchrowski, A.; Kityk, I. V. *Vib. Spectrosc.* **2013**, *64*, 158−163.
(24) Maczka, M.; Paragussu, W.; Freire, P. T. C.; Majchrowski, A.; Pizani, P. S. *J. Phys.: Condens. Matter* **2013**, *25*, 125404.
(25) Liu, S. D.; Zhang, J. J.; Gao, Z. L.; Zhang, S. J.; He, J. L.; Tao, X. T. *Appl. Phys. Express* **2013**, *6*, 042401.
(26) Zhang, J. J.; Zhang, Z. H.; Sun, Y. X.; Zhang, C. Q.; Tao, X. T. *CrystEngComm* **2011**, *13*, 6985−6990.

DOI: 10.1021/cg501574e
Cryst. Growth Des. 2015, 15, 759−763